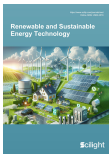
Scilight

Renewable and Sustainable Energy Technology
https://www.sciltp.com/journals/rset



Article

Thermal Performance of a Preheating Chamber for Convective Heating of Aluminum Blocks

Alessandro Montagneretto [1], Matteo Venturelli [1,2,*], Francesco Orlandi [1] and Luca Montorsi [1,2]

[1] Department of Sciences and Methods for Engineering, University of Modena and Reggio Emilia, 42122 Reggio Emilia, Italy
[2] En&Tech—Interdepartmental Center for Industrial Research and Technology Transfer in the Field of Integrated Technologies for Sustainable Development, Efficient Energy Conversion, Building Energy Efficiency, Lighting, and Home Automation, 42122 Reggio Emilia, Italy
* Correspondence: matteo.venturelli@unimore.it

How To Cite: Montagneretto, A.; Venturelli, M.; Orlandi, F.; et al. Thermal Performance of a Preheating Chamber for Convective Heating of Aluminum Blocks. *Renewable and Sustainable Energy Technology* **2026**, *2*(4), 14. https://doi.org/10.53941/rset.2026.100011

Received: 5 June 2026
Revised: 16 October 2026
Accepted: 20 October 2026
Published: 29 October 2026

Abstract: Waste heat recovery is a key strategy for improving the energy efficiency and sustainability of metallurgical processes, in which substantial energy is lost through high-temperature exhaust gases. This study numerically investigates an aluminum-block preheating chamber designed to recover thermal energy from furnace exhaust streams. A three dimensional computational fluid dynamics model was developed to simulate turbulent gas flow and conjugate heat transfer between the exhaust gases and solid aluminum blocks. Two geometric configurations, based on half- and full-block arrangements, and two operating conditions, with the extractor hood open or closed, were compared in terms of flow patterns, temperature distributions, and heat recovery performance. The results demonstrate that both operating conditions and block geometry strongly influence the system's thermal behavior. Enhanced flow mixing promotes heat transfer, while the full-block configuration increases overall thermal energy absorption through greater interaction with the hot gas stream. The optimal configuration produces a substantial increase in block temperature and recovered energy. An economic assessment based on industrial production data estimates annual natural gas savings worth approximately €25,000.

Keywords: CFD analysis; waste heat recovery; energy efficiency; preheating; aluminum industry

1. Introduction

The aluminum industry is a highly energy-intensive process and it uses elevated temperatures throughout with significant environmental impact at all stages. It is estimated that the aluminum industry produces 0.45–0.5 Gt of carbon dioxide (CO_2) equivalent emissions per year [1,2], is responsible for 1% of anthropogenic GHG emissions [3] and 2.5% of CO_2 emissions [4]. Heat recovery technologies can be used to reduce these emissions and also lower fuel and electricity usage. Any reduction in fuel and electricity usage gives a healthier company image of corporate and social responsibility, a reduced CO_2 footprint, sustainability, as well as impacting significantly on profitability.

Aluminum recycling has an important role in reducing the energy consumption and environmental impact associated with aluminum production. Secondary aluminum requires only a fraction of the energy needed for primary production because alumina refining and electrolytic reduction are avoided [5,6]. Nevertheless, scrap remelting remains an energy-intensive operation. Aluminum melting furnaces generally rely on natural gas and discharge a significant amount of thermal energy through high-temperature combustion gases [7–9].

Copyright: © 2026 by the authors. This is an open access article under the terms and conditions of the Creative Commons Attribution (CC BY) license (https://creativecommons.org/licenses/by/4.0/).
Publisher's Note: Scilight stays neutral with regard to jurisdictional claims in published maps and institutional affiliations.

In ref. [10] an extensive review of the different waste heat recovery strategies and their application field have been reported. In recent years, increasing attention has been devoted to advanced WHR technologies, including regenerative systems, organic Rankine cycles (ORC), and thermal energy storage solutions, which can contribute to industrial decarbonization pathways. Examples of the application of Waste heat recovery technologies have been widely adopted in the ceramic industry, where heat pipe based heat exchangers have been used to recover heat from the gases of the ceramic kiln [11,12].

However, these options may require additional equipment, suitable heat users or substantial modifications to an existing plant. An alternative is to use the exhaust gases directly to preheat the material that will subsequently be processed. Since heat is transferred from the flue gas to the incoming load without an intermediate working fluid, direct load preheating can provide a comparatively simple form of heat recovery [8]. Increasing the initial temperature of the aluminum reduces the energy required in the melting furnace and may also shorten the melting cycle. Preheating can additionally remove moisture from the load before it comes into contact with molten metal, thereby reducing the risk of molten-metal splashing [8,13]. Migchielsen and de Groot [9] predicted that the heat loss through flue gas can be reduced from 42.7% to 30.9% with a preheating oven for stacked sow profiles. Preheating scrap to 100 °C prior to charging can reduce cycle times by 8 min [13].

Direct load preheating can be implemented through an unfired section integrated into the furnace, a counter-current arrangement or a separate chamber connected to the exhaust line [8]. In each case, performance depends not only on the temperature of the available gases but also on the interaction between the gas flow and the load. Preferential flow paths may allow part of the gas to pass through the chamber without transferring a significant amount of heat. Conversely, excessive flow concentration may produce local hot spots while leaving other parts of the load at considerably lower temperatures. The geometry of the chamber, the amount and arrangement of material, the available flow passages and the gas velocity must therefore be considered together when designing the system.

Previous studies have demonstrated the potential of waste-heat-assisted material preheating in metallurgical processes. Selvaraj et al. [14] investigated an arrangement in which the heat released by recently cast components was used to preheat metal scrap. Although furnace exhaust gases were not employed, the study showed that direct preheating could produce a measurable reduction in the energy required for melting. The reported energy saving increased from approximately 2.8% for the basic arrangement to 5.7% when aluminum powder was introduced between the casting and the scrap to improve heat transfer. The work demonstrated the practical value of load preheating, but it did not examine the flow distribution or heat-transfer processes occurring inside a flue-gas preheating chamber.

Kangvanskol and Tangthieng [15] considered a preheating chamber for steel slabs installed before a reheating furnace. Exhaust gases leaving the furnace recuperator at approximately 350–450 °C were directed through the chamber before being discharged. Four chamber sizes were evaluated using an energy-balance model, resulting in predicted slab outlet temperatures between approximately 60 and 89 °C and reductions in furnace fuel consumption of 0.94–1.89%. Their analysis highlighted the influence of chamber length and residence time on the recovered energy. However, the adopted modelling approach did not resolve the gas distribution within the chamber or the local temperature field inside the load.

A more closely related investigation was carried out by Arink and Hassan [13], who developed a transient CFD model of an aluminum-scrap preheating furnace supplied by flue gases from three metal-holding furnaces. The inlet conditions were derived from industrial operating data and accounted for variations in both temperature and mass flow rate. The combined exhaust-gas flow fluctuated around 2 kg/s and had an average temperature of approximately 655 °C. The model was used to simulate the heating of stacked aluminum sow profiles and to assess the effects of inlet-flow distribution and partial loading. For a full load of 76 t, the authors predicted that the aluminum could be heated above 200 °C in approximately 200 min.

Despite this earlier work, the behavior of compact external chambers used to preheat stacked aluminum blocks has received limited attention.

The system considered in the present work is installed in an industrial aluminum-processing plant with an annual production of approximately 24,400 t. Aluminum blocks are melted in a natural-gas-fired furnace, and the hot combustion gases leaving the furnace are collected by an extractor hood. Instead of being discharged directly, these gases are conveyed through an external preheating chamber containing the blocks intended for a subsequent melting cycle. The blocks are therefore heated using waste energy from the furnace before being charged and melted in the same production process.

The preheating chamber consists of two consecutive compartments connected through a central opening, with one stack of aluminum blocks placed in each compartment. Exhaust gases enter the first compartment, interact with the first block, pass through the connecting opening and then heat the block located in the second compartment

before leaving the system. Two load arrangements are possible in normal plant operation: a half-block configuration containing seven stacked layers of aluminum and a full-block configuration containing fourteen layers. Increasing the stack height reduces the clearance above the blocks and may force a larger fraction of the gas to flow through the passages between the aluminum layers. At the same time, operation of the extractor hood introduces substantial differences in the inlet temperature, mass flow rate and temporal stability of the exhaust stream.

The present study investigates the combined effects of these geometric and operating variables using a three-dimensional, transient CFD model. The model accounts for turbulent gas flow and conjugate heat transfer between the exhaust gases and the solid aluminum blocks. Four cases are examined by combining the half- and full-block arrangements with open- and closed-hood operating conditions. The inlet boundary conditions are derived from measurements conducted on the industrial installation, while temperatures recorded at selected positions in the aluminum blocks are used to assess the numerical predictions.

This study concerns the analysis of a compact, two-compartment chamber directly integrated with an operating aluminum melting furnace, under conditions in which load height and hood-induced air entrainment simultaneously affect the thermal performance. The study identifies the mechanisms responsible for gas bypass, thermal stratification and unequal heating of the two blocks. It also examines whether a cooler exhaust stream with a higher mass flow rate can provide more effective heating than a hotter but slower flow. Finally, the recovered energy is evaluated against the production scale of the plant to estimate the potential reduction in natural-gas consumption and operating costs.

2. Materials and Methods

2.1. Geometry of the Preheating Chamber

The analyzed system consists of a pre-heating chamber designed to recover thermal energy from exhaust gases and transfer it to aluminum blocks prior to their processing. The following Figure 1 shows the geometry of the considered preheating chamber.

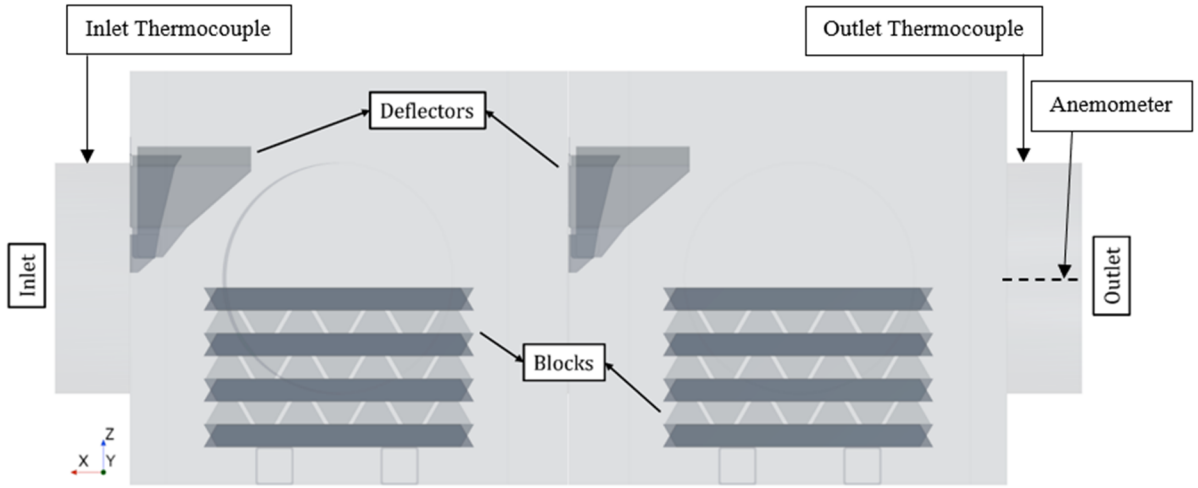


Figure 1. The pre-heating chamber with half blocks.

Hot exhaust gases enter the system through a cylindrical inlet duct of diameter $D = 0.6$ m located in the first chamber (left), and exit through an analogous outlet duct of identical diameter in the second chamber (right). Each chamber features internal dimensions of $La \cdot Lb \cdot Lc$, of 1.2, 1.2 and 1 m respectively. Depending on the configuration, flow deflectors are installed within each chamber to influence the flow distribution and enhance mixing.

Two different block configurations are investigated, and they are shown in Figure 2:

(i) half blocks, consisting of 7 stacked layers of aluminum bricks with total dimensions of $L1 \cdot L2 \cdot L3$ ($0.7 \times 0.7 \times 0.8$ m);

(ii) full blocks, consisting of 14 layers, corresponding to dimensions of $L1 \cdot L2 \cdot 2 \times L3$ due to a doubling in the vertical dimension (Z-axis).

For modeling purposes, each block is treated as a homogeneous solid domain, neglecting the detailed geometry of individual bricks while preserving the overall flow passages between layers. In the case of full blocks, deflectors are removed to reflect the actual industrial configuration, where space constraints prevent their installation.

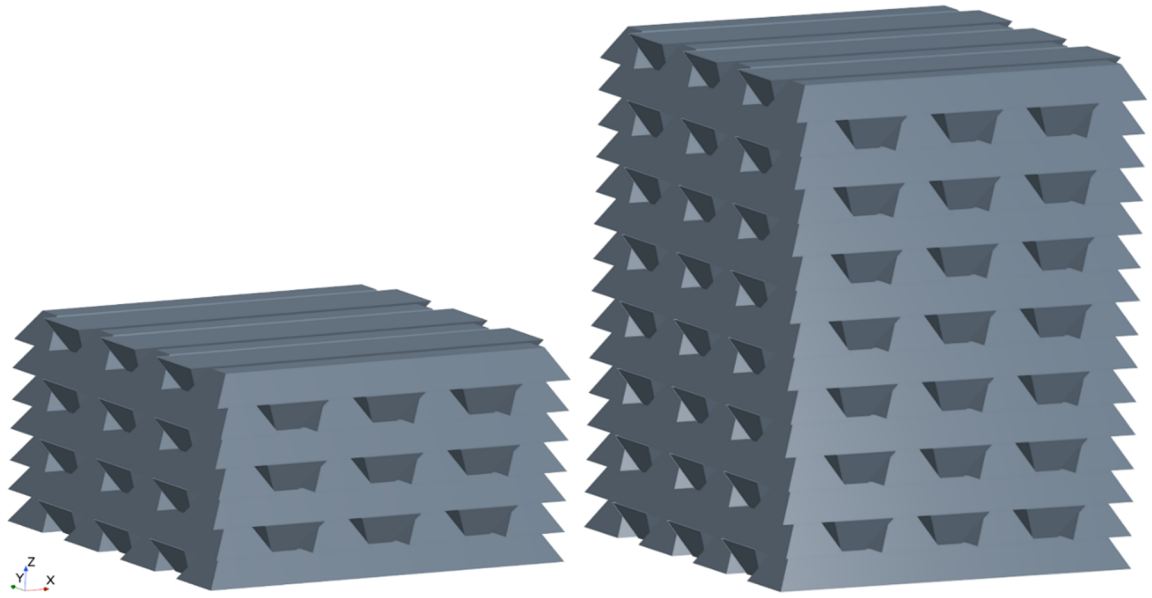


Figure 2. The aluminum blocks: half on the left, full on the right.

2.2. Numerical Modelling

The flow of exhaust gases within the chamber is modeled as a three-dimensional, unsteady, turbulent flow governed by the conservation equations of mass, momentum, and energy, which are considered well-established in the literature.

Turbulence effects are accounted for using the k–ω SST (Shear Stress Transport) model, which combines the robustness of the k–ε model in the free stream with the near-wall accuracy of the k–ω formulation. This approach is particularly suitable for flows characterized by strong gradients, recirculation zones, and flow separation, as expected in the present configuration. To correctly predict the near wall condition the use of the All-y^+ wall treatment was made. This method is an hybrid model that blends between high-y^+ wall functions and low-y^+ wall resolutions depending mainly on the mesh resolution. Being formally adapt to resolve for values $y^+ < 1$ and $y^+ > 30$, it is assured to work correctly even in the buffer zone $1 < y^+ < 30$, leading to an high robustness of this model.

Heat transfer is modeled by solving the energy equation in both fluid and solid domains. The aluminum blocks are treated as solid regions where heat transfer occurs by conduction, while convective heat transfer dominates within the fluid domain.

The interaction between fluid and solid regions is handled through a conjugate heat transfer (CHT) approach, ensuring continuity of heat flux and temperature at the fluid–solid interfaces. This allows accurate prediction of the thermal coupling between the hot gas stream and the aluminum blocks.

Radiative heat transfer is neglected in the present study, assuming that convective heat transfer is the dominant mechanism under the investigated operating conditions.

The computational mesh, shown in Figure 3, is generated using a hybrid approach, with different refinement levels for fluid and solid regions.

For the aluminum blocks, a polyhedral mesh with a base cell size of approximately 1 cm is employed. Given that heat transfer in the solid domain is dominated by conduction, no specific near-wall refinement is required, and a uniform mesh is sufficient to ensure numerical stability.

In the fluid domain, a finer mesh is adopted to accurately resolve the turbulent flow and heat transfer phenomena. A base cell size of 5 cm is used, with local refinements applied at the inlet and outlet sections, as well as near the block surfaces, where strong thermal and velocity gradients are expected. Additional refinement is introduced within the flow passages between block layers to ensure adequate resolution of the convective heat transfer.

Near-wall treatment is handled through prism layers, consisting of two layers with a total thickness equal to approximately 1.5% of the base cell size and a growth factor of 1.5. The final mesh consists of approximately 7 million cells, ensuring a good compromise between accuracy and computational cost.

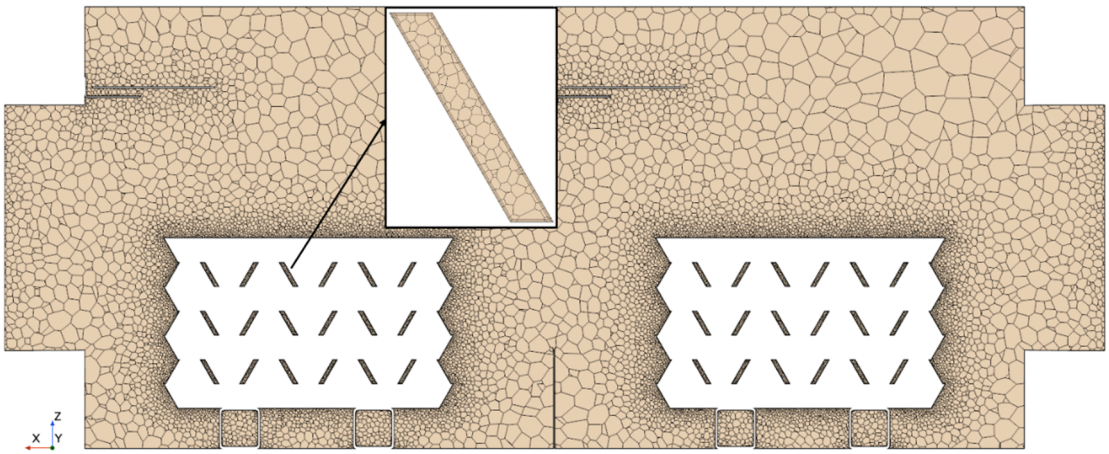


Figure 3. Cross-section of the discretized fluid domain, showing the inlet on the left and the outlet on the right. The zoomed-in view highlights the local polyhedral mesh refinement inside the narrow inter-block gaps.

2.3. Boundary Conditions

Boundary conditions are defined based on experimental measurements acquired at the inlet section of the system. The actual system was monitored with a thermo-couple and an anemometer in order to detect the temperature and the velocity of the exhaust.

The inlet boundary conditions were defined from experimental campaign acquired at sections of the preheating chamber. The exhaust-gas temperature was measured by two thermocouples directly connected to a controller integrated in the preheating chamber. The measurement was performed continuously, with the recorded values being recorded every 30 s. The gas velocity was instead measured using an anemometer. The instrument consists of a steel tube approximately 1 m long, with a probe at its end capable of measuring both the temperature and the velocity of the gas flow. The thermocouples were inserted in the duct upstream and downstream of the pre-heating chamber, exactly at the inlet and outlet sections (Figure 1). The anemometer was inserted perpendicularly to the flow and close to the mid-plane section of the outlet. The measured inlet temperature and velocity were used as input data for the numerical simulation, with the inlet temperature imposed as the gas inlet temperature. The duct diameter is known (60 cm) and the gas velocity is measured, the air mass flow rate was determined from the gas density, which is known as a function of temperature, together with the duct cross-sectional area and the measured velocity. The measured dataset is relatively large, and the recorded values vary over time. The precise trend of the measured temperature and velocity is reported in Figure 4. For each simulated case, the measured inlet temperature was imposed at the inlet boundary, while the measured velocity was used to define the flow condition.

Following the experimental tests conducted on both full and half block configurations, the temperature field within the block itself was monitored using three K-type thermocouples. As illustrated in Figure 5 (magenta dots), these thermocouples were positioned on the top surface, in the central region, and in the lateral zone adjacent to the nearest slot. Unlike the inlet boundary measurements, these local block temperatures were not imposed as boundary conditions; rather, the recorded thermal data were employed as an independent benchmark to validate the numerical model.

The measured steady-state temperature values for both test configurations are summarized in Table 1. Furthermore, a marked thermal asymmetry is observed between the right and left blocks across both configurations.

Table 1. Measured steady-state temperature values via thermocouples.

Configuration	Block	Tbulk [°C]	Tside [°C]	Ttop [°C]
Full Block	Right (DX)	117	110	113
	Left (SX)	110	81	85
Half Block	Right (DX)	119	89	97
	Left (SX)	98	68	91

To mimic the gas surging operated by the fan the inlet condition in the simulation was set as a velocity inlet, with the values of mass flow calculated and temperature corresponding to the values with the probes. The outlet was then set as a pressure outlet. The overall physical simulated time was set as 1 h, with the time step size set as 0.5 s. Lower time step sizes proved no advantage on the precision of the solution, despite the lower values that

would be calculated with means of the Co = 1 condition. As stated previously, two different design conditions are investigated, one with the chamber loaded with half blocks and the other with full blocks, as shown in Figure 2.

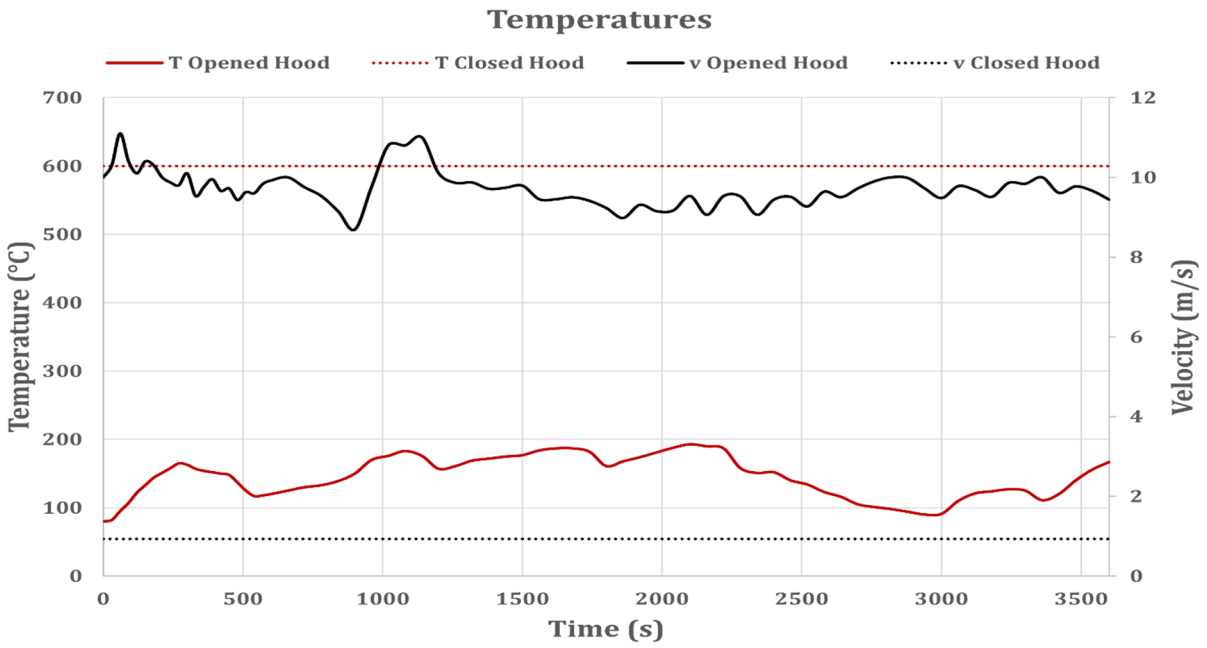


Figure 4. Transient and steady-state inlet profiles for temperature (red) and velocity (black) used as boundary conditions in the CFD model.

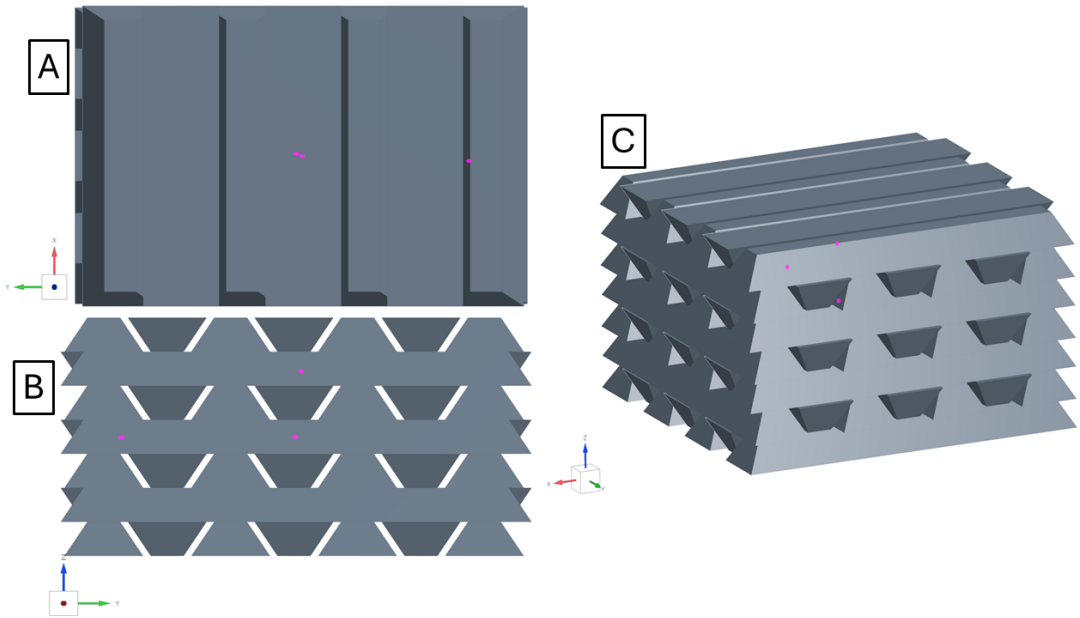


Figure 5. Probes' positions for (**A**) vertical view, (**B**) side view, (**C**) overall view of the half block size.

Additionally, two operating conditions are investigated. These are based on different oven's setting, where the extractor hood placed in the upper part of the oven may be opened or closed. The difference between the configurations lies in the different mass flow and temperature due to the passive air that flows when the extractor hood is opened. In the case of a closed hood the mass flow is lower but constant, being constituted only of the fumes of the combustion, but the temperature is higher, approximately equal as the temperature reached in the oven itself. With an opened hood then the entrained passive air lowers the maximum temperature of the gases and leads to an inconstant mass flow varying during the functioning of the system.

In Table 2 a summary is reported of the simulated cases, along with the minimum, mean, and maximum values of temperature and velocity for the four simulated cases. The table is built on a permutation of the design and operating conditions explained before. The result is a total of 4 simulating cases. All the cases have been run

with segregated flow solver and a first order time solver on a cluster machine with 6 nodes per 52 processors, for a total runtime of 3 days per case.

Table 2. Summary of the simulated cases.

	Blocks	Extractor Hood	T [Min-Med-Max]	V m/s [Min-Med-Max]
A	Half	Opened	82-146-193	8.69-9.73-11.1
B	Half	Closed	600	1
C	Full	Opened	82-146-193	8.69-9.73-11.1
D	Full	Closed	600	1

2.4. Numerical Validation

In order to validate the quality of the set up two analyses were performed in advance before the calculation of the cases as reported in Table 2. These analyses were done to ensure that the generated mesh is sufficiently fine to predict correctly the resolution of the flowing gas in the chamber.

In Figure 6 the wall-y^+ values are reported for a test case of the oven without deflectors. As it can be seen the y^+ values span from the high resolution zone for $y^+ < 1$ and the buffer zone for the rest of the values. As previously stated the All-y^+ wall treatment is assured to be reliable even in the buffer zone, with the only care that few parts of the system may be included in this zone. As it can be assured by looking to Figure 4 the portions of the walls that remain in the buffer zone are evidently lower than the portion included in the safe zone of the higher resolution for $y^+ < 1$. Then, an investigation for the mesh independece as been carried out, including a coarser mesh obtained by a cell base value being 1.5× the value of the chosen mesh, and a finer one having a 0.5× cell base value. To compare the meshes the pressure drop between the inlet and the outlet sections has been monitored, and reported in the subsequent graph

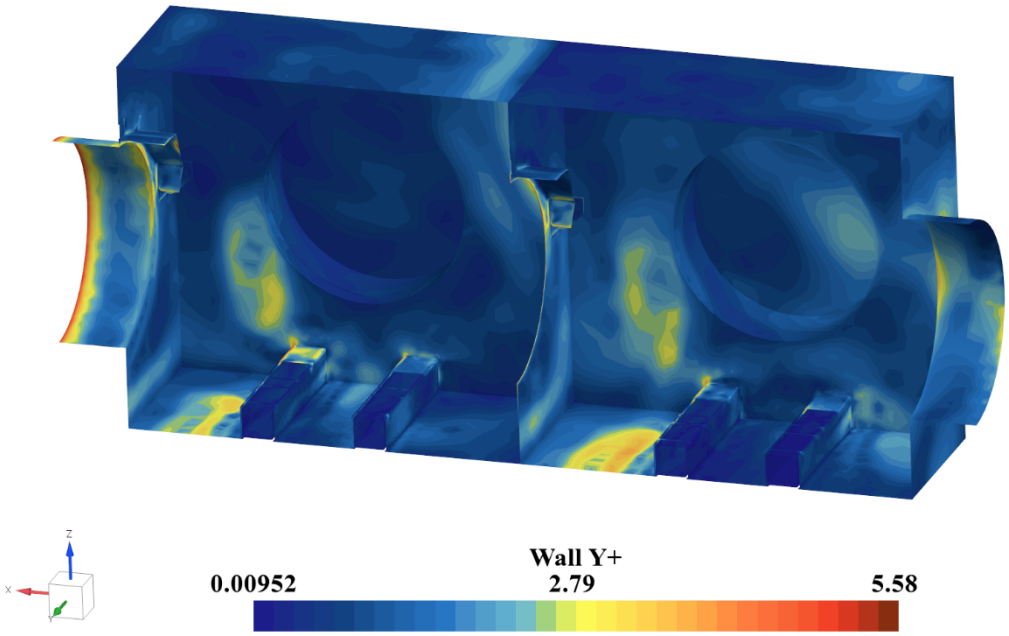


Figure 6. Wall y^+ investigation in the oven walls.

Figure 7 shows that the fine mesh differs for a 4.47% in respect to the value obtained by the standard mesh, which apparently overestimates a little the pressure drop of the system. Being well below a 5% of numerical uncertainty and considering the average $y^+ < 1$ of the wall treatment the standard mesh demonstrates to fit well for the calculation requirements.

Furthermore, case A was chosen as a reference case to test the simulation by monitoring the temperature in the exact locations (side, bulk and top, as in Table 3) where the physical probes were placed. In the simulation case this was accomplished by the generation of 3 different point derived parts, in which the temperature field was monitored during the entire calculation. The results led to the following values.

Table 3. Temperature comparison in probe's location.

	Case A	Simulation	Error
Side probe	68 °C	91.8 °C	~35%
Top probe	91 °C	95.5 °C	~4.9%
Bulk probe	98 °C	101.4 °C	~3.5%

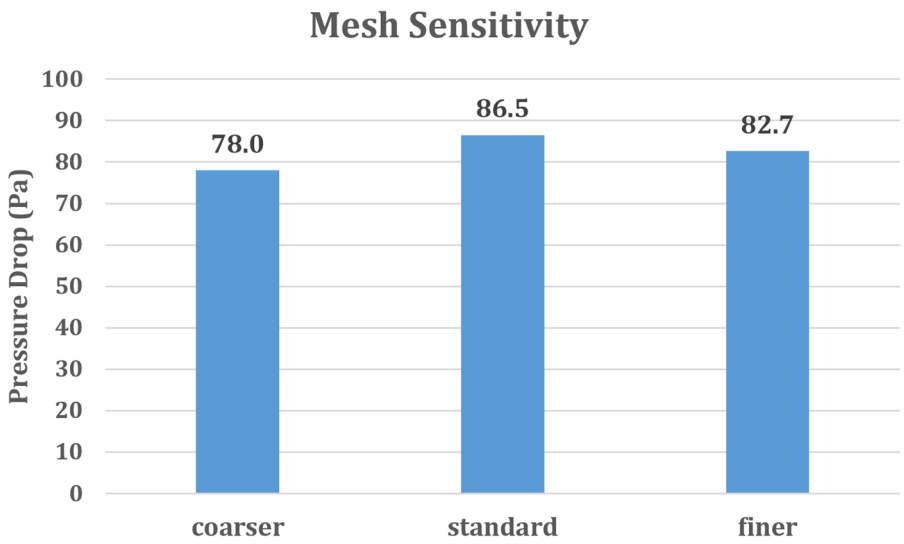


Figure 7. Mesh Sensitivity Analysis results on the pressure drop.

As it can be seen the temperature point values monitored in the numerical probes match coherently and with good approximation. It must be pointed out that the only different value with a considerable margin was found corresponding to the top probe position. As it will be seen by the results, the numerical probe more or less homogeneous values, which is coherent with the temperature field distribution in the chamber, leads to the suspect of an error occurred in the monitoring with that specific probe. Unfortunately, the measurements were done during a single event and no further tests could be carried out. In further tests and simulations this will be investigated further to properly check the temperature measurements.

3. Results

Figure 8 shows the temperature distribution obtained for Case A, corresponding to the half-block configuration with an open extractor hood. The thermal field is characterized by a marked asymmetry between the two chambers. The left chamber, directly exposed to the incoming exhaust gases, reaches relatively uniform temperatures of approximately 160–170 °C, whereas the right chamber is colder and exhibits a broader temperature distribution due to the cooling of the gas after its interaction with the first block.

The incoming hot stream impinges on the upstream face of the left block, generating a high-temperature region concentrated near the upper-left portion of the block surface. The gas then penetrates the channels between the aluminum layers, where heat is progressively transferred to the solid. Consequently, the gas temperature decreases significantly before entering the second chamber and interacting with the right block. Both blocks exhibit a temperature gradient from left to right, although the left block reaches higher average temperatures due to its direct exposure to the incoming flow.

Figure 9 reports the corresponding thermal field for Case B, characterized by the same half-block geometry but with a closed extractor hood. In this case, the inlet gas temperature is significantly higher and more stable than in Case A. As a consequence, the left chamber reaches higher temperatures and a hot plume develops from the inlet region toward the opening connecting the two chambers.

However, despite the higher gas temperature, the aluminum blocks exhibit lower average temperatures than in the open-hood configuration. This behavior indicates that the thermal performance of the system is not governed solely by the inlet temperature, but mainly by the intensity of the convective heat transfer between the gas and the block surfaces.

The closed-hood condition is associated with a lower exhaust gas mass flow rate, since the flow is composed only of combustion products and no additional ambient air is entrained. The reduced mass flow leads to lower gas velocities inside the chamber and, consequently, to a lower convective heat transfer coefficient. As a result, only

a limited fraction of the hot gas effectively penetrates the channels between the aluminum layers, while a significant portion of the thermal energy remains confined in the upper region of the chamber.

Conversely, in Case A the open extractor hood induces passive air entrainment, increasing the overall gas mass flow rate through the chamber. Although the resulting gas temperature is lower, the larger flow rate produces higher velocities within the passages between the aluminum layers. This enhances forced convection and promotes stronger interaction between the hot gas and the solid surfaces, leading to more effective heat transfer and higher average block temperatures.

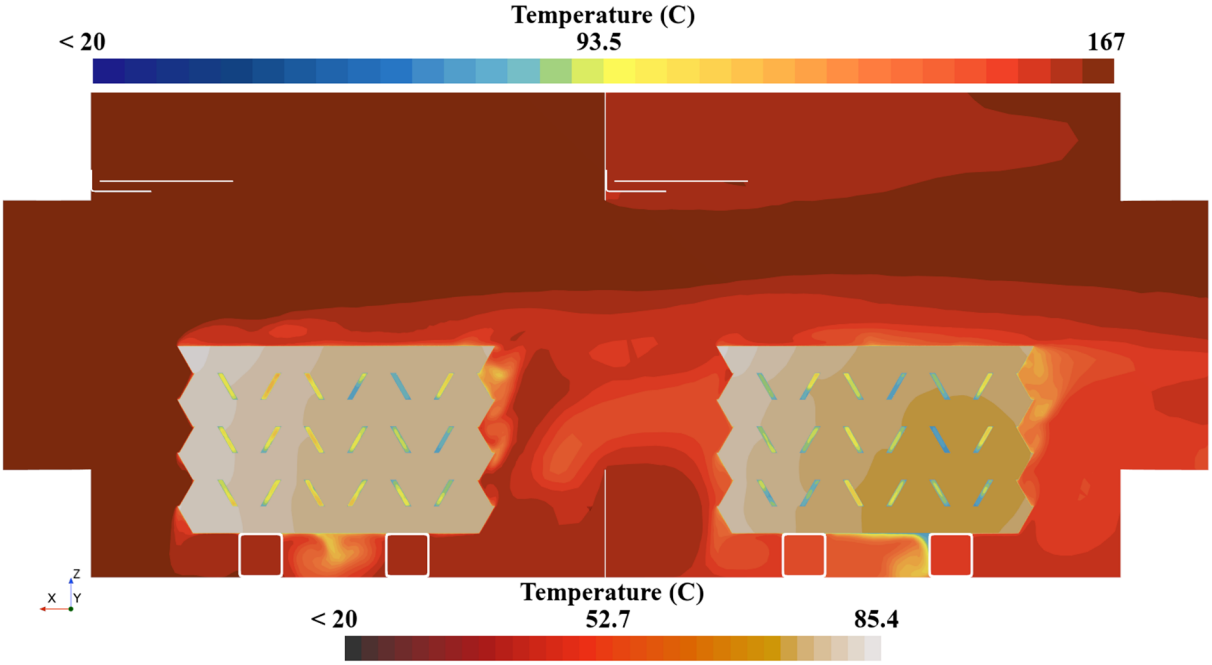


Figure 8. Temperature field section for the open-hood case with half-block configuration, showing separate Temperature scalar colour-bar for the fluid region (top scale) and the solid aluminum blocks (bottom scale).

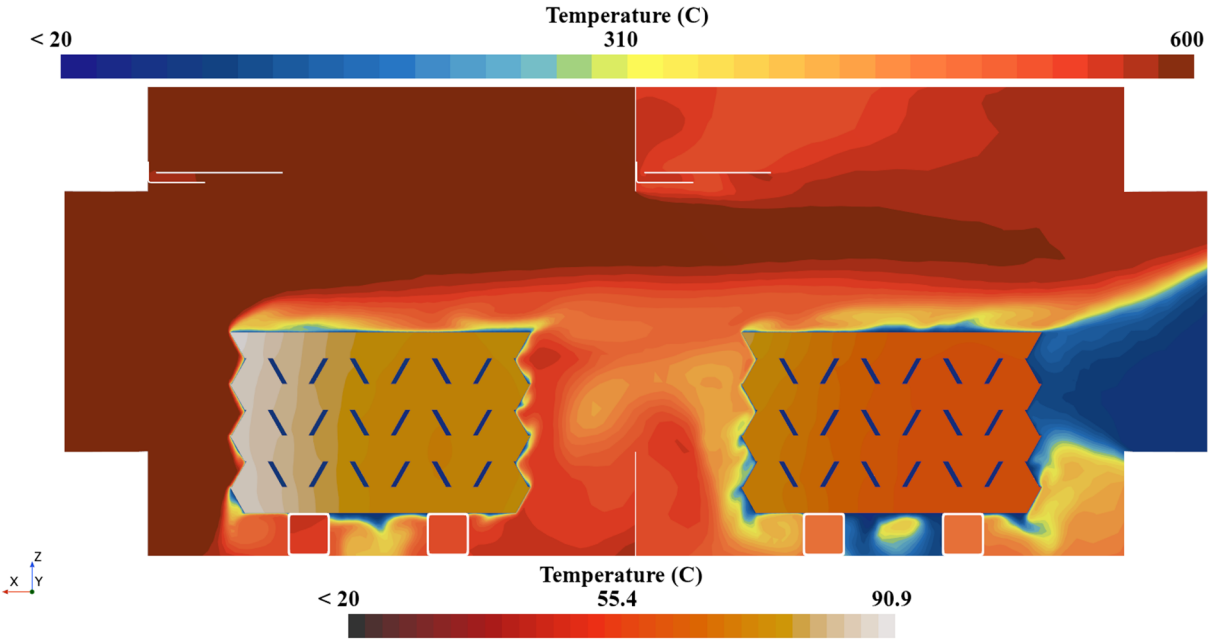


Figure 9. Temperature field section for the close-hood case with half-block configuration, showing separate Temperature scalar colour-bar for the fluid region (top scale) and the solid aluminum blocks (bottom scale).

The comparison between Cases A and B also highlights the importance of the geometric “step effect” associated with the half-block configuration. Due to the relatively large free volume above the blocks, the incoming gas stream tends to detach from the upper surface of the left block and propagate directly toward the outlet. This phenomenon reduces the amount of thermal energy transferred to the lower portion of the chamber and to the

downstream block. The effect is particularly pronounced in Case B, where the combination of lower flow velocity and larger free volume promotes thermal stratification and flow bypass, resulting in significantly lower temperatures in the second block.

The effect of block geometry can be assessed by comparing the half-block and full-block configurations under the same operating conditions. Figures 10 and 11 show the temperature distributions obtained for Cases C and D, corresponding to the full-block arrangement with open and closed extractor hood, respectively.

In both cases, the increase in block height substantially modifies the flow field inside the chamber. Compared with the half-block configuration, the free volume above the blocks is strongly reduced and the incoming gas stream is forced to flow through the passages between the aluminum layers rather than bypassing the solid region. As a consequence, the interaction between the hot gas and the blocks is enhanced, leading to higher and more uniform temperatures.

For the open-hood condition (Case C, Figure 10), the temperature field appears relatively homogeneous in both chambers. The left chamber remains slightly hotter than the right one, with an average difference of approximately 30 °C, but the temperature distribution around the two blocks is significantly more uniform than in the corresponding half-block case. In particular, the two blocks reach nearly identical average temperatures.

The more uniform thermal field indicates that the increase in gas mass flow rate associated with the open hood, combined with the reduced free space above the blocks, promotes stronger mixing and more effective forced convection inside the block channels. Unlike the half-block configuration, no pronounced hot stream develops in the upper part of the chamber, since the reduced clearance limits the occurrence of flow detachment and bypass. Most of the thermal energy is therefore directly transferred to the solid.

Figure 11 shows the temperature distribution for Case D, corresponding to the full-block configuration with closed extractor hood. Compared with Case B, the increase in block size strongly mitigates the thermal stratification previously observed in the upper region of the chamber. The hot stream is no longer confined to a narrow path above the left block, but instead spreads more uniformly through the chamber and around both blocks.

Although the gas mass flow rate remains lower than in the open-hood case, the reduction of the available flow area produces locally higher velocities within the passages between the aluminum layers. This increases the convective heat transfer coefficient and partially compensates for the lower overall mass flow rate. Consequently, both blocks reach substantially higher temperatures than in the corresponding half-block configuration.

Nevertheless, Case D still exhibits lower block temperatures than Case C. This confirms that the gas mass flow rate remains the dominant parameter governing the heat transfer process. The higher inlet temperature associated with the closed hood is not sufficient to compensate for the lower gas velocity and the resulting reduction in convective heat transfer.

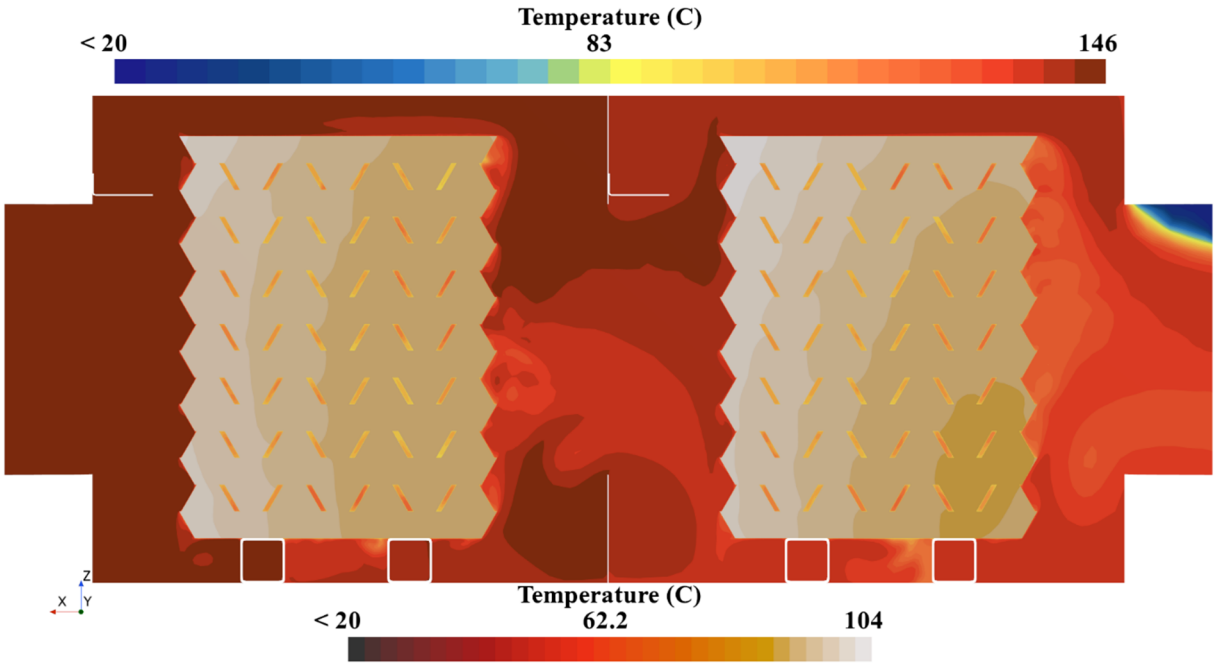


Figure 10. Temperature Section for the full block opened hood case with full-block configuration, showing separate Temperature scalar colour-bar for the fluid region (top scale) and the solid aluminum blocks (bottom scale).

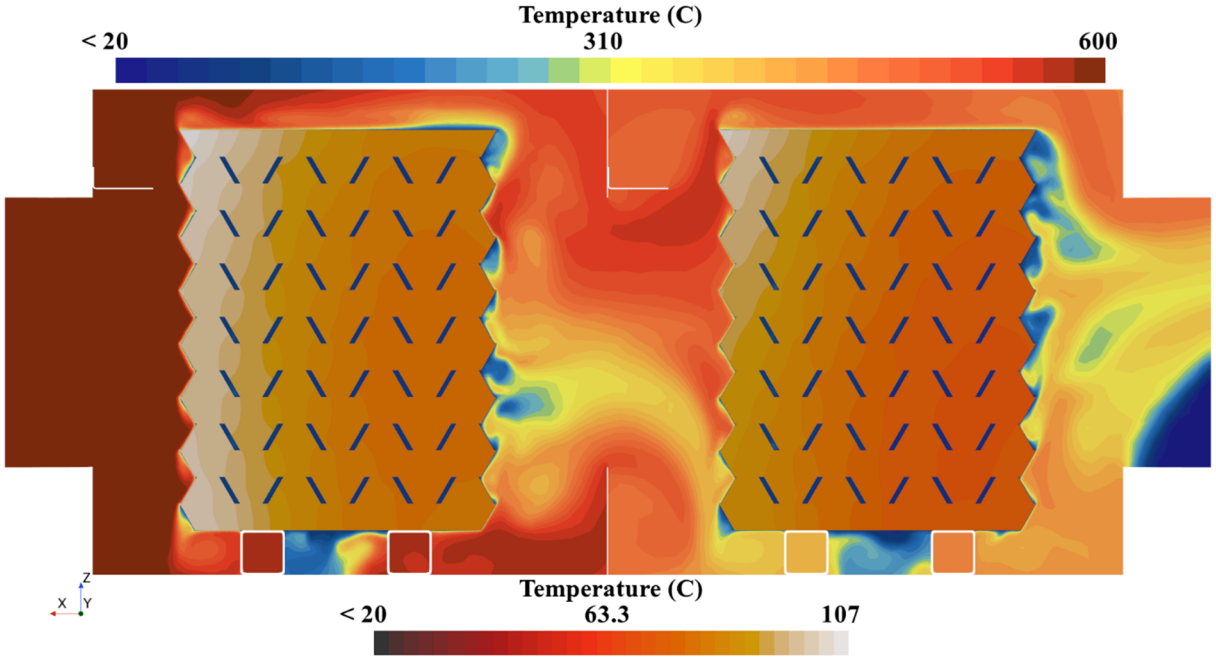


Figure 11. Temperature Section for the full block closed hood case with full-block configuration, showing separate Temperature scalar colour-bar for the fluid region (top scale) and the solid aluminum blocks (bottom scale).

The average volumetric temperatures reported in Figure 12 further support these observations. For all cases, the upstream block reaches slightly higher temperatures than the downstream one because it is directly exposed to the incoming hot gas. However, the temperature difference between the two blocks decreases significantly when moving from the half-block to the full-block configuration. In particular, Case C exhibits nearly identical temperatures for both blocks, demonstrating that the full-block arrangement leads to a more effective distribution of thermal energy throughout the chamber.

Further insight can be obtained from the average thermal powers transferred to the blocks, shown in Figure 13. The full-block configurations are characterized by significantly larger heat transfer rates than the half-block cases, especially for the upstream block. This is a direct consequence of the larger exchange surface and the higher gas velocities induced by the reduced flow area.

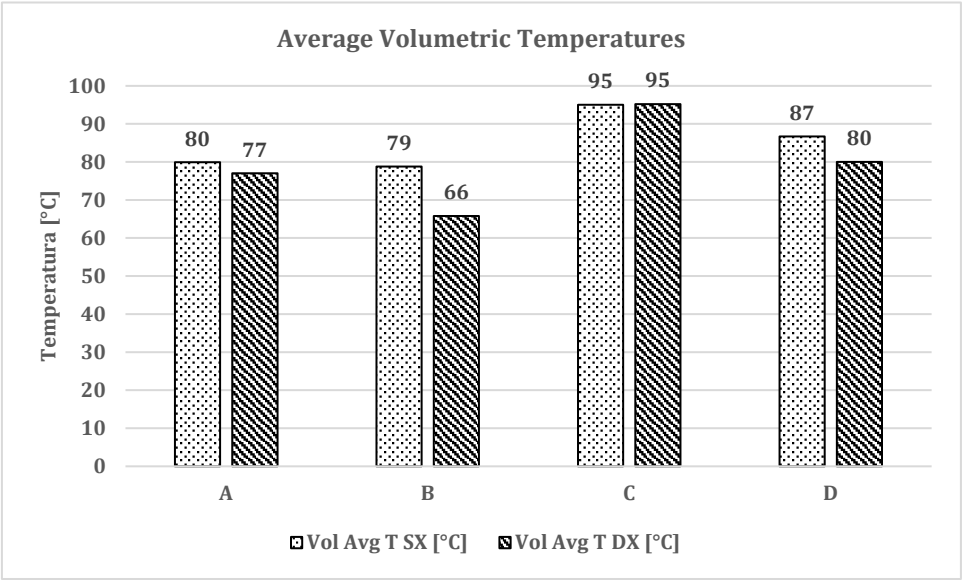


Figure 12. Comparison of average volumetric block temperatures across the simulated cases (A–D) for the left (SX) and right (DX) positions.

For a given block geometry, the average heat transfer rates are relatively similar for open and closed hood conditions. Therefore, the higher final temperatures observed in Cases A and C are mainly attributable to the larger gas mass flow rate and to the more effective convective heat transfer maintained throughout the entire heating

period. Among all the investigated cases, the combination of full blocks and open extractor hood (Case C) provides the best thermal performance, yielding the highest and most uniform temperatures together with the largest amount of recovered thermal energy.

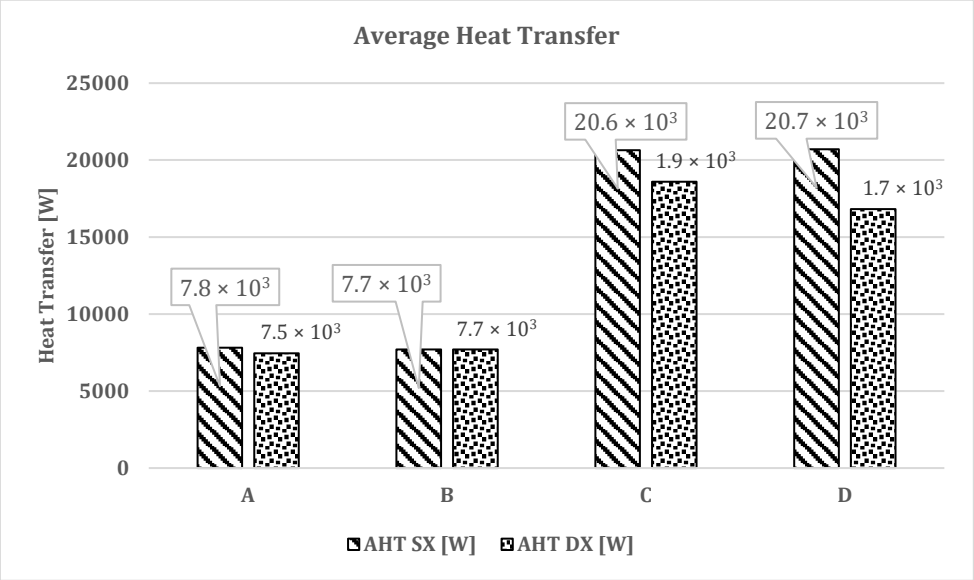


Figure 13. Average heat transfer rate (thermal power) absorbed by the blocks for each simulated case (A–D), comparing left (SX) and right (DX) positions.

4. Economic Estimation

To evaluate the practical relevance of the proposed pre-heating system, a preliminary economic assessment was performed considering the thermal energy recovered in the most favorable configuration, namely Case C (full blocks with open extractor hood).

According to the numerical results, this configuration leads to the highest average block temperature after one hour of pre-heating. Starting from an initial temperature of 20 °C, the aluminum blocks reach an average final temperature close to 95 °C, corresponding to an average temperature increase of approximately 75 °C.

The thermal energy stored in the blocks can be estimated as:

$$Q = m \cdot c_p \cdot \Delta T$$

where (m) is the total mass of the aluminum blocks, (c_p) is the specific heat capacity of aluminum, and (ΔT) is the average temperature rise.

Assuming the actual mass, i.e., 450 kg, loaded in the preheating chamber and an average specific heat capacity of aluminum equal to 0.90 kJ/kg K, the total amount of thermal energy recovered during one pre-heating cycle is approximately 29.7 MJ, corresponding to 8.26 kWh.

This recovered energy directly reduces the amount of fuel required in the downstream melting or heating process. Thus, it is possible to estimate a thermal energy absorbed by one ton of aluminum equal to approximately 18.35 kWh.

Assuming that the furnace is fueled by natural gas, the corresponding fuel saving can be estimated using the lower heating value of methane. By considering an average lower heating value equal to 9.9 kWh/Sm^3, the recovered thermal energy translates into a reduction of approximately 1.85 Sm^3 of natural gas per ton of processed material.

For an industrial production rate of 24,400 t/year, the annual natural gas saving is therefore 45,140 Sm^3/year, resulting in more than 18 k€ of annual saving for the natural gas purchase. In addition to this, the avoided cost for the CO_2 is approximately 7000 €. The overall beneficial reduction in the operating cost is approximately 25 k€.

Although a detailed investment analysis is beyond the scope of the present work, the obtained annual savings suggest that the payback period of the system would likely be relatively short, especially considering the simple geometry and passive operation of the chamber. Indeed, a reasonable estimation of the investment cost is approximately 50 k€, obtaining a payback period around 2 years. This confirms that the proposed solution is not only thermally effective, but also economically attractive for industrial implementation. All of the input parameters, physical properties, and economic assumptions used for the assessment are summarized in Table 4.

Table 4. Summary of input parameters, physical properties, and calculated economic outcomes for the Case C pre-heating configuration.

Parameter/Variable	Value	Unit
Aluminum Specific Heat Capacity (c_p)	0.90	kJ/kg K
Natural Gas Lower Heating Value (LHV)	9.9	kWh/Sm^3
Recovered Energy per Cycle (Q)	29.7 (8.26)	MJ (kWh)
Specific Energy Recovery	18.35	kWh/t
Specific Natural Gas Savings	1.85	Sm^3/t
Annual Production Rate	24,400	t/year
Annual Natural Gas Savings	45,140	Sm^3/year
Annual Natural Gas Purchase Savings	>18,000	€/year
Annual Avoided CO_2 Cost	~7000	€/year
Total Annual Operating Cost Reduction	~25,000	€/year
Estimated Investment Cost (CAPEX)	~50,000	€
Estimated Payback Period	~2	years

5. Conclusions

A three-dimensional CFD analysis of an industrial pre-heating chamber for aluminum blocks has been presented in this work. The study investigated the combined effect of block geometry and operating conditions on the thermal performance of the system, with the aim of maximizing the recovery of waste heat from furnace exhaust gases.

Four different configurations were analyzed by combining two block arrangements (half and full blocks) with two operating conditions corresponding to open and closed extractor hood configurations. The numerical model included turbulent flow and conjugate heat transfer between the exhaust gases and the aluminum blocks.

The obtained results highlight that the thermal performance of the system is governed primarily by the convective heat transfer coefficient rather than by the inlet gas temperature alone. Although the closed-hood configuration is characterized by higher gas temperatures, the associated lower mass flow rate leads to lower gas velocities and therefore to a reduced convective heat transfer coefficient. Conversely, the open-hood condition, despite its lower inlet temperature, promotes higher gas velocities and stronger mixing within the chamber, resulting in more effective heat transfer to the aluminum blocks.

The geometry of the blocks was also found to play a crucial role. The half-block configuration allows the development of a bypass flow above the blocks, reducing the interaction between the hot gas and the solid surfaces. In contrast, the full-block configuration reduces the free volume within the chamber and forces the gas to flow through the passages between the aluminum layers. This suppresses the flow bypass effect, enhances the convective heat transfer coefficient, and produces a more uniform thermal field.

Among the investigated cases, the configuration consisting of full blocks and open extractor hood (Case C) provided the best overall performance. This case yielded the highest average block temperatures, the most uniform thermal distribution, and the largest heat transfer rate between the gas and the solid. Under these conditions, the average temperature of the aluminum blocks increased from approximately 20 °C to about 95 °C after one hour of pre-heating.

A preliminary economic assessment showed that the recovered thermal energy corresponds to approximately 18.35 kWh per ton of processed aluminum, leading to a reduction in natural gas consumption of about 26,600 Sm^3/year for the considered production capacity. This translates into an annual cost saving of approximately €22,000 and an estimated reduction of about 53 tCO_2/year.

Overall, the results demonstrate that the proposed pre-heating chamber represents an effective and economically attractive solution for waste heat recovery in the aluminum industry. The study also confirms the usefulness of CFD as a design and optimization tool for industrial thermal systems.

Future developments of the work may include the experimental validation of the numerical model, the inclusion of radiative heat transfer effects, and the investigation of alternative chamber geometries and block arrangements aimed at further improving heat recovery efficiency.

Author Contributions

A.M.: writing, validation; M.V.: conceptualization, methodology, writing, reviewing and editing; F.O.: software, original draft preparation; L.M.: supervision. All authors have read and agreed to the published version of the manuscript.

Funding

This research received no external funding.

Institutional Review Board Statement

Not applicable.

Informed Consent Statement

Not applicable.

Data Availability Statement

The data analyzed during the current study are not publicly available due to confidentiality agreement between participants.

Conflicts of Interest

The authors declare no conflict of interest.

Use of AI and AI-Assisted Technologies

No AI tools were utilized for this paper.

References

1. Menzie, W.D.; Barry, J.J.; Bleiwas, D.I.; et al. *The Global Flow of Aluminum from 2006 through 2025*; Open-File Report 2010–1256; U.S. Geological Survey: Reston, VA, USA, 2010; pp. 1–60. https://doi.org/10.3133/ofr20101256.
2. Das, S. Achieving Carbon Neutrality in the Global Aluminum Industry. *JOM* **2012**, *64*, 285–290. https://doi.org/10.1007/s11837-012-0237-0.
3. Luo, Z.; Soria, A. *Prospective Study of the World Aluminium Industry*; EUR 22951 EN; Publications Office of the European Union: Luxembourg, 2008. https://doi.org/10.2791/36024.
4. Steinfeld, A. High-Temperature Solar Thermochemistry for CO_2 Mitigation in the Extractive Metallurgical Industry. *Energy* **1997**, *22*, 311–316. https://doi.org/10.1016/s0360-5442(96)00103-x.
5. Raabe, D.; Ponge, D.; Uggowitzer, P.J.; et al. Making Sustainable Aluminum by Recycling Scrap: The Science of "Dirty" Alloys. *Prog. Mater. Sci.* **2022**, *128*, 100947. https://doi.org/10.1016/j.pmatsci.2022.100947.
6. Dardor, D.; Flórez-Orrego, D.; Germanier, R.; et al. Decarbonizing the Aluminium Industry: A Comprehensive Review of Pathways and Process Integration Perspectives. *Energy Strategy Rev.* **2025**, *61*, 101853. https://doi.org/10.1016/j.esr.2025.101853.
7. Brough, D.; Jouhara, H. The Aluminium Industry: A Review on State-of-the-Art Technologies, Environmental Impacts and Possibilities for Waste Heat Recovery. *Int. J. Thermofluids* **2020**, *1–2*, 100007. https://doi.org/10.1016/j.ijft.2019.100007.
8. U.S. Department of Energy. Load Preheating Using Flue Gases from a Fuel-Fired Heating System. Process Heating Tip Sheet No. 9, Industrial Technologies Program. 2006. Available online: https://www.energy.gov/sites/prod/files/2014/05/f16/load_preheating.pdf (accessed on 5 February 2026).
9. Migchielsen, J.M.; de Groot, J.D. Design Considerations for Charge Preheating Ovens. In Proceedings of the Light Metals 2006, San Antonio, TX, USA, 12–16 March 2006; p. 737.
10. Jouhara, H.; Khordehgah, N.; Almahmoud, S.; et al. Waste Heat Recovery Technologies and Applications. *Therm. Sci. Eng. Prog.* **2018**, *6*, 268–289. https://doi.org/10.1016/j.tsep.2018.04.017.
11. Venturelli, M.; Brough, D.; Milani, M.; et al. Comprehensive Numerical Model for the Analysis of Potential Heat Recovery Solutions in a Ceramic Industry. *Int. J. Thermofluids* **2021**, *10*, 100080. https://doi.org/10.1016/j.ijft.2021.100080.
12. Jouhara, H.; Bertrand, D.; Axcell, B.; et al. Investigation on a Full-Scale Heat Pipe Heat Exchanger in the Ceramics Industry for Waste Heat Recovery. *Energy* **2021**, *223*, 120037. https://doi.org/10.1016/j.energy.2021.120037.
13. Arink, T.; Hassan, M.I. Metal Scrap Preheating Using Flue Gas Waste Heat. *Energy Procedia* **2017**, *105*, 4788–4795. https://doi.org/10.1016/j.egypro.2017.03.945.
14. Selvaraj, J.; Varun, V.S.; Vignesh; et al. Waste Heat Recovery from Metal Casting and Scrap Preheating Using Recovered Heat. *Procedia Eng.* **2014**, *97*, 267–276. https://doi.org/10.1016/j.proeng.2014.12.250.
15. Kangvanskol, K.; Tangthieng, C. An Energy Analysis of a Slab Preheating Chamber for a Reheating Furnace. *Eng. J.* **2014**, *18*, 1–12. https://doi.org/10.4186/ej.2014.18.2.1.